Intrinsic phototransduction persists in melanopsin-expressing ganglion cells lacking diacylglycerol-sensitive TRPC channel subunits

Claudio E. Perez-Leighton[1,*], **Tiffany M. Schmidt**[1,*], **Joel Abramowitz**[2], **Lutz Birnbaumer**[2], and **Paulo Kofuji**[1]

[1] Department of Neuroscience, University of Minnesota, Minneapolis, Minnesota

[2] Laboratory of Neurobiology, Division of Intramural Research, National Institute of Environmental Health Sciences, National Institutes of Health

Abstract

In mammals, intrinsically photosensitive retinal ganglion cells (ipRGCs) mediate various non-image-forming photic responses such as circadian photoentrainment, pupillary light reflex, and pineal melatonin suppression. ipRGCs directly respond to environmental light by activation of the photopigment melanopsin followed by the opening of an unidentified cation-selective channel. Studies in heterologous expression systems and in the native retina have strongly implicated diacylglycerol-sensitive transient receptor potential channels containing TRPC3, TRPC6, and TRPC7 subunits in melanopsin-evoked depolarization. Here we show that melanopsin-evoked electrical responses largely persist in ipRGCs recorded from early postnatal (P6-P8) and adult (P22-P50) mice lacking expression of functional TRPC3, TRPC6, or TRPC7 subunits. Multielectrode array recordings performed at P6-P8 stages under conditions that prevent influences from rod/cone photoreceptors show comparable light sensitivity for the melanopsin-evoked responses in these mutant mouse lines in comparison to wild-type mice. Patch-clamp recordings from adult mouse ipRGCs lacking TRPC3 or TRPC7 subunits show intrinsic light-evoked responses equivalent to those recorded in wild-type mice. Persistence of intrinsic light-evoked responses was also noted in ipRGCs lacking TRPC6 subunits, however of significantly smaller magnitudes. These results demonstrate that the melanopsin-evoked depolarization in ipRGCs is not mediated by either TRPC3, TRPC6, or TRPC7 channel subunits alone. They also suggest that the melanopsin signaling pathway includes TRPC6-containing heteromeric channels in mature retinas.

Keywords

intrinsically photosensitive ganglion cell; circadian entrainment; retina; mouse

INTRODUCTION

Intrinsically photosensitive retinal ganglion cells (ipRGC) express the photopigment melanopsin (Opn4) and respond directly to light with a sustained depolarization and increase in intracellular calcium (Berson *et al.*, 2002; Hattar *et al.*, 2002; Sekaran *et al.*, 2003;

Address for correspondence: Paulo Kofuji, Department of Neuroscience, University of Minnesota, 6-145 Jackson Hall, 321 Church Street SE, Minneapolis, MN 55455., kofuj001@umn.edu. Phone: (612) 625-6457. FAX: (612) 626-5009.
*Equal contribution

Hartwick *et al.*, 2007). ipRGCs densely innervate brain areas related to non-image-forming (NIF) photic responses (Hattar *et al.*, 2006; Baver *et al.*, 2008). These cells integrate light information from rod and cone photoreceptors with their intrinsic light response (Dacey *et al.*, 2005; Schmidt *et al.*, 2008; Schmidt & Kofuji, 2010a), and their axonal projections are the main source of photic input to elicit various NIF visual behaviors (Goz *et al.*, 2008; Guler *et al.*, 2008; Hatori *et al.*, 2008).

It has been suggested that mammalian ipRGCs and *Drosophila* rhabdomeric photoreceptors share similar phototransduction mechanisms (Berson, 2007; Peirson *et al.*, 2007). Sequence analysis of Opn4 has indicated its closer evolutionary relationship to invertebrate rhodopsins than vertebrate opsins (Nickle & Robinson, 2007). Like ipRGCs, *Drosophila* photoreceptors depolarize in response to light (Hardie & Raghu, 2001). Additionally, as in *Drosophila* photoreceptors (Hardie & Raghu, 2001), ipRGC phototransduction engages a membrane-anchored mechanism and requires activation of a $G_{q/11}$ protein and phospholipase-C activity (Graham *et al.*, 2008). However, identification of the channel(s) that mediate the melanopsin-evoked depolarization in ipRGCs remains elusive (Do & Yau, 2010).

In *Drosophila* photoreceptors, the transient receptor potential (TRP) channel mediates the initial depolarization upon light stimulation (Hardie & Minke, 1992; Phillips *et al.*, 1992). There are seven mammalian TRP homologues, denominated TRP canonical (TRPC) subunits 1–7 (Clapham *et al.*, 2001) that combine to form tetrameric channels (Hofmann *et al.*, 2002). Pharmacological evidence implicates the diacylglycerol-sensitive TRPC channels (formed by different combinations of subunits TRPC3, TRPC6 and TRPC7), in ipRGC intrinsic phototransduction. However, evidence has been contradictory with regard to which of these TRPC subunits are involved (Warren *et al.*, 2006; Hartwick *et al.*, 2007; Sekaran *et al.*, 2007). Furthermore, immunocytochemical evidence has been scarce, but supports cellular colocalization of melanopsin with TRPC6 and possibly TRPC7 (Warren *et al.* 2006; Sekaran *et al.* 2007). Messenger RNA analysis of ipRGC-enriched primary cultures has also indicated the presence of all three subunits and enrichment of TRPC7 (Hartwick *et al.*, 2007). Finally, the melanopsin photopigment can trigger activation of TRPC3 channels in various heterologous expression systems (Panda *et al.*, 2005; Qiu *et al.*, 2005).

Perhaps the greatest hurdle in identifying whether and which TRPC channel subunits are involved in melanopsin phototransduction *in situ* is the lack of pharmacological tools specifically affecting individual TRPC channels (Birnbaumer, 2009). Because of this lack of specificity of various TRPC inhibitors, we utilized mouse lines lacking either TRPC3, TRPC6 or TRPC7 subunits to examine the role of these TRPC subunits in ipRGC phototransduction. By means of multielectrode array (MEA) and single cell patch-clamp recordings, we demonstrate that melanopsin-evoked responses of ipRGCs are not mediated by TRPC3, TRPC6, or TRPC7 subunits as homomeric channels. Our data also suggest that TRPC6 subunits contribute to the nonselective cation conductance mediating the ipRGC intrinsic photoresponse.

MATERIALS AND METHODS

Animals

TRPC3−/− (Hartmann *et al.*, 2008), *TRPC6−/−* (Dietrich *et al.*, 2005), and *TRPC7−/−* lines in 129Sv:C57BL/6J background (see next section) were backcrossed to the Opn4-EGFP mouse line (Schmidt *et al.*, 2008) for electrophysiological recordings. The Opn4-EGFP mice in a C57BL/6J background have been described previously (Schmidt *et al.*, 2008) and were used as wild-type controls as well. The *Opn4−/−* mouse line (Hattar *et al.*, 2002) was generously provided to us by Dr. King-Wai Yau. Animals were cared for in accordance with guidelines described in *Guide for the Care and Use of Laboratory Animals*,

using protocols approved by the University of Minnesota Institutional Care and Use Committee.

Generation of *TRPC7−/−* mice

TRPC7−/− mice were generated by disrupting the *Trpc7* gene in a four step process. First, the targeting vector containing loxP sites flanking exon 5 and the PGK-neo cassette was generated (Figure 2). Second, in embryonic stem cells (ES) cells, loxP recombination sites were introduced by homologous recombination into the introns bordering exon 5 of the murine *Trpc7* gene. Electroporation and isolation of neomycin resistant cell clones were performed as described (Rudolph *et al.*, 1994). Third, the F0 generation of chimeric mice generated from blastocysts that had received the targeted ES cells were interbred and used to generate mice homozygous for the *Trpc7* gene with floxed exon 5 (*Trpc7* flx/flx). Fourth, male *Trpc7* flx/flx mice were crossed to female mice carrying a transgene directing the expression of Cre recombinase under the control of the Sox2 promoter (Tg[Sox2-Cre] mice, Jackson Laboratories, Bar Harbor, ME, USA). The resulting heterozygous null mice were bred and mice which were *TRPC7−/−* and negative for the Sox2-Cre transgene were identified by PCR analysis of tail biopsies (Figure 2).

RNA extraction and reverse transcription

Retinas from postnatal P6-P8 animals were dissected in 95% O_2-5% CO_2 bicarbonate buffered Ames' medium (Sigma, St. Louis, MO, USA) at room temperature and stored in RNALater (Qiagen, Valencia, CA, USA) at −80°C. RNA was extracted using RNeasy kit (Qiagen) and immediately quantified using Nanodrop 1000 spectrophotometer (Thermo Scientific, Wilmington, DE, USA). Equal amounts of RNA for all samples were subjected to reverse transcription using Quantitect Reverse Transcription Kit (Qiagen) and cDNA stored at −20°C until use.

Real time Polymerase Chain reaction (PCR)

Real Time PCR was conducted on the cDNA from WT, *TRPC3−/−*, *TRPC6−/−*, and *TRPC7−/−* retinal samples employing the TaqMan system (Roche Applied Science, Indianapolis, IN, USA) in a LightCycler 2.0 Thermocycler (Roche Applied Science). All primers used were designed using the Universal Probe Library Assay Design Center and were: β-actin (fwd: 5'-AAGGCCAACCGTGAAAAGAT-3, rev: 5'-GTGGTACGACCAGAGGCATAC-3), TRPC3 (fwd: 5'-TGGATTGCACCTTGTAGCAG-3', rev: 5'-ACCCAGAAAGATGATGAAGGAG-3'), TRPC6 (fwd: 5'-TACTGGTGTGCTCCTTGCAG-3', rev: 5'-CAAACTTCATGAACGGTCCTC-3'), TRPC7 (fwd: 5'-GTGGCCTACTTCACCTACGC-3', rev: 5'-CGAGATGATCTGGGGGTCT-3') and Opn4 (fwd:5'-CTCTCTGTTAGCCCCACGAC-3',rev:5'-GACATCGACTGTGGGGAAG-3'). Opn4, TRPC3, TRPC6 and TRPC7 mRNA levels were normalized against β-actin mRNA levels correcting by PCR efficiencies determined by the dilution curve method (Pfaffl, 2001).

End Point PCR

Primers for murine TRPC3 exon 7 (fwd: 5'-AGTGACTTCTGTTGTCCTCA-3', rev: 5'-CTCGATCTCTTGGTATGAGCTA-3'), murine TRPC6 exon 7 (fwd: 5'-TGGGACCCTACTGATCCTCAGA-3', rev: 5'-ATGCTTCATTCTGTTTTGCGCC-3'), murine TRPC7 exon 5 (fwd: 5'-GGACAAACCCTGAGGAGCCC-3', rev: 5'-TTAACGCCCTCAAACCGGTCG-3') were designed using Perl scripts. PCR reactions were performed using HotStart Taq Plus DNA polymerase kit (Qiagen). PCR protocol

consisted of 5 min at 95°C followed by 30 cycles of 1 min at 94°C, 30 sec at 58°C, and 1 min at 72°C. Extension was concluded at 72°C for 10 min.

Immunohistochemistry

Immunocytochemistry was performed essentially as previously described (Connors & Kofuji, 2002; Schmidt *et al.*, 2008). The primary antibodies used in this study as well as their dilutions are listed in Table 1. We used goat anti-mouse AlexaFluor (AF) 488 (A11029), goat anti-rabbit AF488 (A11034) and donkey anti-mouse AF594 (A11058) as secondary antibodies (all from Invitrogen, Carlsbad, CA, USA). Controls with omission of either primary or secondary antibodies revealed no detectable signal. In addition, the localization and morphology of the stained cells with each primary antibody matched previous descriptions in retina (Haverkamp & Wassle, 2000) and see Table 1, confirming the specificity of the antibodies used in this study. For the anti-melanopsin antibody, its specificity was tested upon immunostaining of WT and *Opn4−/−* retinas. Staining of a subset of wide-field ganglion cells in the ganglion cell layer in WT retinas, and lack of staining in the Opn4−/− retinas shows that the antibody labels ipRGCs specifically (Supplementary Figure 1).

Image Observation and ipRGC cell count

All fluorescent specimens were imaged with an Olympus Fluoview1000 confocal microscope. For the retinal markers and melanopsin cell count, we used 40X (N.A. 1.3) and 20X (N.A. 0.85) oil-immersion lens respectively. Optical sections were collectedat 0.2- to 1.0-μm intervals and reconstructions of severaloptical images onto a single plane were performed using NationalInstitutes of Health ImageJ 1.42q (http://rsb.info.nih.gov/ij/). Contrast and brightness of the images for retinal markers were adjusted using Adobe Photoshop CS2 (Adobe System, San Jose, CA, USA). For melanopsin cell density analysis, all images were processed with Adobe Photoshop CS2 (Adobe System). Images were converted to their negative to observe dark stained nuclei. The image levels and contrast were adjusted to match a standard image. This step assigned the same contrast level to all the images to make easier the identification of stained nuclei. Dark melanopsin immunoreactive nuclei were counted semi automatically using ImageJ Cell Counter plugin (http://rsbweb.nih.gov/ij/plugins/cell-counter.html). Averages from 4–5 images from each retina were used to calculate cell density for each retina. Opn4 cell density data was analyzed using the R Statistical Project v2.11 software (http://www.R-project.org) with a one-factor ANOVA with genotype as experimental factor. Significance criterion was set at 0.05.

MEA Recordings: Data recording

Retinas of P6-P8 animals were dissected as described (Schmidt *et al.*, 2008; Schmidt & Kofuji, 2010b) and mounted ganglion cell layer down over the MEA electrode array. The electrodes were arranged in a 8X8 grid with no corner electrodes, 200 μm inter-electrode spacing, and 30 μm electrode diameter. The MEA system was purchased from Multi Channel Systems (Reutlingen, Germany) and included the 60-electrode array (200/30-Ti), headstage (MEA1060-2-BC), filter amplifier (FA60SBC) and PCI-bus data acquisition system (MCCard 64). Retinas were dark adapted for 15–20 minutes before start of the light stimulation protocol. During all recordings retinas were superfused with 95% O_2-5%CO_2 bicarbonate buffered Ames' medium (Sigma) with synaptic blockers at 36°C. Data recorded was amplified and digitized with a sampling frequency of 25 kHz.

MEA Recordings: Light Stimulation

Stimulation protocol consisted of 1 min baseline in the dark, 1 min light stimulation (480 nm, narrow band pass filter), and 4 min post-stimulation in the dark. Light stimulation was generated using a Xenon lamp feeding a fiber optic to the preparation interposed with a filter wheel fitted with neutral-density and narrow band-pass filters (ChromaTechnologies, Rockingham, VT, USA). We used light intensities (in photons / $cm^2 \cdot sec$) of 7.32×10^{10}, 2.31×10^{11}, 7.32×10^{11}, 1.16×10^{12}, 2.31×10^{12}, 3.67×10^{12}, 7.32×10^{12}, 3.67×10^{13}, 7.32×10^{13} as measured with a calibrated radiometer model S370 (UDT Instruments,San Diego, CA, USA).

MEA Recordings: Data analysis

MEA data was processed using high (200 Hz) and low (3000 Hz) band pass filters. Extracellular spikes were extracted using a threshold filter of -4.5 standard deviations calculated independently for each electrode using MCRack v 4.0.0 software (Multi Channel Systems). Extracted spikes from all light intensities corresponding to a single electrode were concatenated into a single file using MCData Tool v2.6.0 software (Multi Channel Systems). Only electrodes that showed at least twice the number of spikes during the light stimulation period than during baseline were used for further analysis. Spikes were aligned to reduce jitter and clustered using principal component analysis with Offline Sorter v 2.8.6 software (Plexon Inc, Dallas, TX, USA). ipRGC light responses were identified based on the time lock between light stimulation and the appearance of spikes. ipRGC response features were further analyzed using Igor Pro 5.04 software (WaveMetrics, Portland, OR, USA) and the extracted features were: 1) IR_{50} of the light response, defined after fitting a Hill function to the number of light induced spikes normalized to maximum versus the log of light intensity (log (IR)), 2) Light induced spikes, defined as the total number of spikes during light stimulation, 3) Maximal spiking frequency, defined as the maximal spiking frequency after light onset using 5 second bins, 4) Latency, defined as time between light onset and maximal spiking frequency.

MEA Recordings: Statistical Analysis

Initial analysis ipRGC intrinsic light responses showed the data had non-normality, lack of homocedasticity and unequal sample size. Therefore, we decided to use randomization tests for the analysis of the data (Edgington & Onghena, 2007). We analyzed the IR_{50} with a randomization-based t-test to compare directly between each TRPC$-/-$ and WT responses followed by a false discovery rate (FDR) correction for multiple testing. We analyzed the dose response curves between each TRPC$-/-$ and WT by means of a randomization 2-way ANOVA using genotype (TRPC$-/-$ vs WT) and light intensity as experimental factors. Pairwise comparisons between genotypes at each light intensity were done by t-test using the residual error of the ANOVA as variance followed by an FDR correction. We analyzed the number of light induced spikes and other features of the ipRGC intrinsic light response using a randomization t-test followed by a FDR correction for each of the comparison between WT and TRPC responses at each of the light intensities. All statistical analyses were implemented using the R Statistical Project v2.11 software (http://www.R-project.org). We generated all graphs using the R Statistical Project Software. For all tests the significance criterion was set at 0.05. Data are shown as mean ± SEM.

MEA Recordings: Pharmacology

Synaptic blocker cocktail added to the extracellular Ames' medium included: 250 μM DL-2-amino-4-phosphonobutyrate (DL-AP4, a group III metabotropic glutamate receptor agonist); 10 μM 6,7-dinitroquinoxaline (DNQX, α-amino-3-hydroxy-5-methyl-4-isoxazolepropionic acid (AMPA)/kainate receptor antagonist); 0.3 μM strychnine, 50 μM picrotoxin, and 10 nM

(±)-epibatidine dihydrochloride. All reagents were purchased from Tocris (Ellesville, MO, USA).

Whole-cell Patch Clamp Recordings

Recordings were performed on P 22–50 animals from the Opn4-EGFP mouse line described previously (Schmidt & Kofuji, 2009; 2010b) on a WT, *TRPC3−/−, TRPC6−/−, or TRPC7−/−* background. Dissections were performed as described previously (Schmidt *et al.*, 2008; Schmidt & Kofuji, 2010b). Retinas were removed from the eyecups and bubbled with 95% O_2-5% CO_2 bicarbonate buffered Ames' solution (Sigma) at room temperature in a dark room with minimal ambient light. Prior to recording, retinas were treated with Ames' solution containing collagenase/hyaluronidase (240 and 1000 U/ml, respectively) at room temperature for 15 minutes to remove vitreous. Recordings were performed using an Axon 700B Amplifier (Molecular Devices, Union City, CA) with extracellular solution containing 95% O_2-5% CO_2 bicarbonate buffered Ames' solution (Sigma) at 32–34°C. For current clamp recordings, pipettes were filled with (in mM): 125 K-gluconate, 2 $CaCl_2$, 2 $MgCl_2$, 10 EGTA, 10 HEPES, 0.5 NaGTP, and 2 Na_2ATP, pH to 7.2 with KOH. For voltage clamp recordings, pipettes were filled with (in mM): 125 CsMethanesulfonate, 10 $CsCl_2$, 5 EGTA, 1 $MgCl_2$, 2 Na_2ATP, 10 NaHepes, 10 Phosphocreatine, 2 QX314, 0.5 NaGTP, pH to 7.6 with KOH. Intracellular solutions also contained 10 μM Alexafluor-594 hydrazide (AF-594) (Invitrogen) and dendritic stratification was classified by focusing in the proximal and distal layers of the IPL. Series resistance was noted in all recordings, but uncompensated and only recordings with series resistance of < 30 MΩ were included for analysis. For whole cell recordings, the synaptic blocker cocktail was identical to that employed in the MEA recordings (see above) but without the cholinergic blocker epibatidine dihydrochloride. We also included 0.5 μM tetrodotoxin (TTX, sodium channel blocker) (Ascent, Princeton, NJ, USA) to prevent action potential firing.

Whole cell patch clamp recordings: Light stimulation

A filter wheel fitted with various narrow bandpass (10 nm bandwidth) and neutral-density filters (Chroma Technologies, Rockingham, VT) and shutter (Lambda-3, Sutter Instruments, Novato, CA, USA) was used to control the intensity and duration of light stimuli. Light stimuli for all experiments were full-field, 480 nm light (5.87 X 10^{16} photons.cm^{-2}.s^{-1} unattenuated) generated by interposing a narrow bandpass filter. Stimuli were delivered using a xenon lamp feeding the camera port at −2.1LogI for current clamp and −1.5LogI for voltage clamp experiments. Cells were given 5 min to dark adapt prior to light stimulation.

Whole cell patch clamp: Analysis

Whole cell currents were analyzed off-line with Clampfit (Molecular Devices), and membrane potential values were measured from raw traces over a 1 s sliding time window to maximize the signal to noise ratio using Igor Pro 6.0 (Portland, OR, USA). Resting membrane potential (Vm) values were calculated by taking the average membrane voltage of the first 10 s of baseline prior to any light stimulation.

Whole cell patch clamp: Statistics

Statistical analysis of whole-cell data was performed using Origin 7.5 (OriginLab, Northampton, MA, USA). Statistical comparison of means was performed using a two-tailed Student's t-test or one way *Analysis of Variance* (*ANOVA*) and significance criterion was set at 0.05. Data are presented as mean ± SE.

RESULTS

MEA analysis suggests two subtypes of ipRGC light responses in WT mice

We first examined the light-evoked responses of ipRGC in isolated retinas of WT mice using MEA recordings. We chose to record from early postnatal mice (P6-P8) as it has been shown that ipRGCs constitute the only light-responsive ganglion cells at this developmental stage (Sekaran *et al.*, 2005; Tu *et al.*, 2005) allowing for isolated recording of ipRGC intrinsic light responses. Though outer retinal signaling to ganglion cells is not present at this developmental stage (Sernagor *et al.*, 2001), we included a cocktail of synaptic blockers in the Ames' medium to inhibit any glutamatergic, GABAergic, and glycinergic signaling to ipRGCs (see Methods). This ensured that all light responses recorded originated from ipRGC intrinsic photoresponses. We also added cholinergic blockers to minimize interference from retinal waves present at this developmental stage (Sun *et al.*, 2008). The MEA technique allowed for simultaneous recording of light responses from multiple ipRGCs per retina. Following a period of dark adaptation for 15–20 min, the retinas were submitted to diffuse, uniform light stimulation of increasing irradiance (from 7.3×10^{10} to 7.3×10^{13} photons / $cm^2 \cdot$ sec) for 60 sec at 480 nm, the peak wavelength for melanopsin activation (Berson, 2007; Do & Yau, 2010). The retinas were then allowed to readapt to dark for 4 min following each stimulation episode. Figure 1A shows the light induced spike activity from ipRGCs of two apparently distinct subtypes (see below). Similar to previous studies, we observed that all ipRGCs responded to increasing light intensities with increasing firing rates that reached their maximum several seconds following light onset. Upon termination of the light stimulus, most ipRGCs continued to display substantial spike activity that persisted for several seconds. The relatively sluggish initiation and termination of spike responses are consistent with previous reports of melanopsin-evoked light responses (Berson *et al.*, 2002; Dacey *et al.*, 2005; Tu *et al.*, 2005; Schmidt *et al.*, 2008). Spike discharge rates returned to baseline 5–30 seconds following light offset (Figure 1A).

Previous studies have demonstrated considerable heterogeneity in the sensitivity, response latency, and maximal spike frequency of melanopsin-evoked light responses (Sekaran *et al.*, 2003; Sekaran *et al.*, 2005; Tu *et al.*, 2005; Schmidt & Kofuji, 2009). Likewise we found that ipRGCs could be qualitatively separated into subpopulations with high and low light sensitivities (LS), consistent with previous reports at this developmental stage (Tu *et al.* 2005). Figure 1A shows representative voltage traces from a high (Figure 1A, left) and a low (Figure 1A, right) LS ipRGC. The $logIR_{50}$ histogram of the normalized ipRGC intrinsic light responses ($n = 93$ cells, from 5 retinas) showed an apparent bimodal distribution (Figure 1B) that could be arbitrarily separated into high ($n = 66$ cells) and low ($n = 27$ cells) LS cell populations using a cutoff of $log(IR) = 12.70$ photons / $cm^2 \cdot$ sec (Figure 1B–C). We also found that high LS ipRGCs had significantly higher average spike frequency and maximal spike frequency as well as a significantly shorter latency to response onset than low LS ipRGCs (Table 2).

Generation of *TRPC7−/−* mouse line

To examine the contribution of the diacylglycerol-sensitive TRPC channel subunits to the melanopsin-mediated light responses we utilized *TRPC3−/−*, *TRPC6−/−* and *TRPC7−/−* mouse lines. The generation of the *TRPC3−/−* and *TRPC6−/−* mouse lines has been described elsewhere (Dietrich *et al.*, 2005; Hartmann *et al.*, 2008). To generate *TRPC7−/−* mice, the TRPC7 gene was ablated in mice through homologous recombination using a targeting construct to delete the exon 5 within the putative 4th transmembrane domain (Figure 2A). The deletion of exon 5 was catalyzed by Cre-recombinase and verified by PCR analyses of genomic DNA (Figure 2A, B). In addition, RT-PCR analyses of transcripts from brain WT and *TRPC7−/−* mice confirm the deletion of exon 5 at mRNA level (Figure 2C,

D). The *TRPC7−/ −* mouse line was viable and showed no obvious differences from WT in weight and size.

TRPC3−/ −, TRPC6−/ − and *TRPC7−/ −* mouse retinas develop normally

To examine whether diacylglycerol-sensitive TRPC channels are expressed at early postnatal stages in the mouse retina, we performed real-time RT-PCR on P6-P8 mouse retinas. We found evidence for the expression of TRPC3, TRPC6, and TRPC7 at this developmental stage, with higher levels for the TRPC3 subunit (Supplementary Figure 2). End-point RT-PCR analysis also detects expression of these subunits in WT retinas at adult stages, in agreement with previous reports. (Warren *et al.*, 2006; Hartwick *et al.*, 2007; Sekaran *et al.*, 2007). As expected, the transcripts of exons deleted by genetic targeting were not detectable by end-point RT-PCR in *TRPC3−/ −, TRPC6−/ −,*and *TRPC7−/ −* mouse retinas (Figure 3A). We next asked whether the lack of expression for these TRPC channel subunits affected the overall development of the retinas as TRPC channels have been implicated in guidance of nerve growth cones (Li *et al.*, 2005) and in neuronal development (Tai *et al.*, 2009). DAPI nuclear staining showed no apparent abnormalities in the nuclear layers in the retinas of any of the mutant mouse lines (Figure 3B). Furthermore, immunohistochemical analysis of Müller cells, rod bipolar cells, dopaminergic amacrine cells and cholinergic amacrine cells yielded no observable differences between WT and mutant mice (Supplementary Figure 3). Analysis of Opn4 immunoreactive cells revealed no differences in ipRGC cell density between genotypes (Figure 2C, one-way ANOVA, $F_{3,28} = 0.422$, $P = 0.736$). These results suggest that lack of expression of TRPC 3/6/7 channel subunits does not affect the morphological development of the retinal cell types and ipRGCs.

Early postnatal *WT, TRPC3−/ −, TRPC6−/ −,* and *TRPC7−/ −* ipRGCs have similar intrinsic light responses

To examine whether TRPC3, TRPC6, and TRPC7 subunits participate in melanopsin-evoked phototransduction, we next performed MEA recordings of ipRGC light responses from *TRPC3−/ −, TRPC6−/ −* and *TRPC7−/ −* mice using the same stimulation protocols as those employed in the WT mice. For these experiments we used P6-P8 retinas from *TRPC3−/ −* ($n = 83$ cells from 5 retinas), *TRPC6−/ −* ($n = 50$ cells from 3 retinas) and *TRPC7−/ −* ($n = 38$ cells from 3 retinas) mice. ipRGCs from *TRPC3−/ −, TRPC6−/ −,* and *TRPC 7−/ −* mice responded to light stimulation with similar overall characteristics as WT ipRGCs (Figure 4). At lower light intensities, the initiation of responses was relatively sluggish and spike activity persisted for several seconds following light-offset. Figure 4 shows voltage traces for a typical cell from *TRPC3−/ −* (Figure 4A), *TRPC6−/ −* (Figure 4B), and *TRPC7−/ −* (Figure 4C) retinas. The persistence of light responses in these mutant mice indicates that the individual expression of TRPC3, TRPC6, or TRPC7 subunits is not required for melanopsin-driven photoresponses. Though we were able to separate WT ipRGCs into two subpopulations of high- and low-sensitivity groups based on a bimodal distribution of IR_{50} (see above), the distribution of IR_{50}'s in the TRPC$−/ −$ mice, especially *TRPC7−/ −* mice, did not show an apparent bimodal distribution. Thus we considered all ipRGCs as a homogeneous population for further comparison between the mouse lines. Figure 5A,C, E shows the histograms for the $\log(IR_{50})$ distributions for the TRPC $−/ −$ retinas. Analysis of the $\log(IR_{50})$ values (in photons / $cm^2 \cdot sec$) using a randomization t-test followed by a FDR multiple testing correction (See Methods) showed no differences between WT (12.5 ± 0.05) and *TRPC3−/ −* (12.7 ± 0.05, $t_{175} = 1.848$, $P = 0.096$), *TRPC6−/ −* (12.4 ± 0.06, $t_{140} = 1.505$, $P = 0.133$) and *TRPC7−/ −* (12.4 ± 0.05, $t_{128} = 2.209$, $P = 0.094$). Next, we compared the dose-response curve between WT and each TRPC$−/ −$ by means of a randomization based two-way ANOVA with genotype and light intensity as experimental factors. The statistical analysis showed no significant differences between WT

and *TRPC3 −/ −* (Figure 5B) or *TRPC6 −/ −* (Figure 5D). Pairwise comparisons at each light intensity between WT and *TRPC7 −/ −* showed only significant differences at 2 light intensities in the middle of the dose-response curve (Figure 5F). Together, this evidence shows that ipRGCs from all three TRPC −/ − mice maintain their intrinsic light responses with similar light sensitivity compared to the WT mice.

The previous results indicate that the light sensitivity of the melanopsin phototransduction pathway is not appreciably altered upon genetic inactivation of TRPC3, TRPC6 or TRPC7 channels. Next we tested whether the light-evoked spike output of the ipRGCs is modified in these mouse lines. We compared the average light-evoked spike frequency of ipRGCs in WT, *TRPC3 −/ −*, *TRPC6 −/ −*, and *TRPC7 −/ −* mice at various light intensities (Figure 6). We did not observe a statistically significant difference in firing frequency for either *TRPC6 −/ −* or *TRPC7 −/ −* ipRGCs with the exception of an enhanced spike activity in the *TRPC6 −/ −* mouse at one light intensity (See Methods for details on statistical analyses). However, we observed a small but significant decrease in the firing frequency of *TRPC3 −/ −* ipRGCs at most light intensities tested, indicating that ipRGCs in *TRPC3 −/ −* mice, though they display similar sensitivity to ipRGCs in the WT mouse, do not attain similar spike frequencies in response to light stimulation (See Figure 6 legend for details).

Persistence of intrinsic light-evoked responses in M1 and M2 ipRGCs recorded from TRPC3 −/ − TRPC6 −/ −, and TRPC7 −/ − adult mice

One potential limitation of MEA recordings is that they sample only light responding ipRGCs. If genetic inactivation of a TRPC channel subunit renders subpopulations of ipRGCs unresponsive to light then they would escape detection using this method. In addition, MEA recordings are unable to identify the ipRGC subtype using morphological criteria. There are at least three and perhaps as many as five major subtypes of ipRGCs based on their morphological and physiological characteristics (Viney *et al.*, 2007; Schmidt *et al.*, 2008; Ecker *et al.*, 2010). To allow for identification of and recording from single ipRGCs in the various TRPC knockout lines, we crossed our Opn4-EGFP reporter mouse line with the *TRPC3 −/ −*, *TRPC6 −/ −*, and *TRPC7 −/ −* mouse lines. At adult stages, ipRGCs subtypes can be recognized based on their pattern of dendritic stratification in the inner plexiform layer (IPL) (Viney *et al.*, 2007; Schmidt *et al.*, 2008; Schmidt & Kofuji, 2009). M1 cells have dendrites branching in the outermost layers of the IPL while the M2 cells have dendrites branching in the innermost layers of the IPL (Schmidt *et al.*, 2008). When we recorded intrinsic light responses of M1 and M2 cells to full-field, bright, 480 nm light in WT and *TRPC6 −/ −* mice in current clamp mode, we found that all ipRGCs in the TRPC6 −/ − mice responded to light stimulation, but with a significantly reduced amplitude (maximum depolarization) (M1 = 7.24 ± 1.30 mV, $n = 12$; M2 = 2.77 ± 0.16 mV, $n = 9$) relative to WT (M1 = 24.57 ± 1.67 mV, $n = 9$, $t_{19} = 8.31$, $P = 0$, two-tailed *t*-test; M2 = 5.77 ± 0.45 mV, $n = 10$, $t_{17} = 6.45$, $P = 0.00001$, two-tailed *t*-test)(Figure 7A, B, and E). Similar results were obtained when light responses of WT and TRPC6 −/ − M1 and M2 cells were recorded in voltage clamp mode with ipRGCs in TRPC6 −/ − mice all responding to light, but with significantly smaller inward current (maximum current) (M1 = −149.28 ± 31.51 pA, $n = 14$; M2 = −37.9 ± 10.50 pA, $n = 12$) than that of WT ipRGCs (M1 = −524.50 ± 54.10 pA, n = 11, $t_{23} = −6.30$, $P = 0$, two-tailed *t*-test; M2 = −82.79 ± 0.85 pA, $n = 11$, $t_{21} = −2.97$, $P = 0.0073$, two-tailed *t*-test)(Figure 7C, D, and F). ipRGCs in *TRPC3 −/ −* (M1 = −347.65 ± 99.25 pA, n = 6; M2 = −53.62 ± 2.30 pA, $n = 4$) and *TRPC7 −/ −* (M1 = −337.47 ± 48.75 pA, $n = 3$; M2 = −64.57 ± 26.6 pA, $n = 4$) also all responded to light with a sustained inward current similar to that seen in WT (M1 = −415.91 ± 42.53 pA, $n = 7$, $F_{2,13} = 0.34$, $P = 0.72$, one-way *ANOVA* M2 = −44.51 ± 8.61 pA, $n = 5$, $F_{2,10} = 0.44$, $P = 0.65$, one-way *ANOVA*) (Figure 8A–C) . Collectively, these results support our results using MEA and indicate that ipRGCs continue to respond to light in the absence of TRPC3, TRPC6, or

TRPC7 subunits. Furthermore, data from *TRPC6−/−* mice indicate that this subunit may play a significant role in melanopsin phototransduction for both M1 and M2 cells.

DISCUSSION

Using a combination of MEA and whole-cell electrophysiological recordings from retinas of various TRPC knockout mouse lines, we demonstrate that genetic inactivation of either TRPC3, TRPC6, and TRPC7 channel subunits does not ablate intrinsic light-evoked responses in melanopsin-expressing ganglion cells at early postnatal (P6-P8) or adult (P22-P50) stages. A key finding of this study is the persistence of intrinsic light-evoked responses in ipRGCs in all tested TRPC knockout lines. At early postnatal stages, we found no differences in the irradiance-response curves between *TRPC3−/−* and *TRPC6−/−* and only a small change in the slope of *TRPC7−/−* compared to WT ipRGC responses. In addition, we only detected a small decrease in the spike output for the *TRPC3−/−* ipRGCs. At the moment it is unclear whether these rather subtle effects on *TRPC3−/− and TRPC7−/−* ipRGCs at early postnatal stages reflect a modest role of these subunits in melanopsin-evoked phototransduction or they reflect strain-related variations in genetic background (see methods). In adult mouse retinas, the melanopsin-evoked light responses were largely unaltered in the *TRPC3−/−* and *TRPC7−/−* in both M1 and M2 cells. However, consistent diminished melanopsin-mediated photoresponses were noted in *TRPC6−/−* retinas for both ipRGC subtypes. No major developmental abnormalities were observed in the TRPC knockout mouse retinas, which contained similar numbers of melanopsin-expressing ganglion cells and cytoarchitecture similar to WT retinas.

Previous MEA studies of ipRGCs in mice and chicks have revealed different types of light responses supporting the existence of ipRGC subtypes in early postnatal and adult retinas (Tu *et al.*, 2005; Neumann *et al.*, 2008). However another study failed to reveal the heterogeneity of light responses in adult rat (Weng *et al.*, 2009). In our study, two types of ipRGC responses were present at P6-P8 based on the apparent bimodal distribution of ipRGC light sensitivities. Contrary to previous studies, (Tu *et al.*, 2005; Neumann *et al.*, 2008) our analysis did not reveal a third functional subtype of ipRGCs at this age. While it is possible that technical factors in the preparation of the sample or the recording conditions may account for this discrepancy, we do not have a consistent explanation for this difference between our and previous analysis (Tu *et al.*, 2005; Neumann *et al.*, 2008). Interestingly, the apparent bimodal distribution of light sensitivities of ipRGCs was less well defined in the mutant mouse lines. It is tempting to speculate that lack of expression of TRPC channels altered the functional properties or development of one specific ipRGC subtype but we do not have data to support that conclusion at this time.

Several lines of evidence are suggestive that the photopigment melanopsin is at least capable of activating diacylglycerol-sensitive TRPC channels formed by subunits TRPC3, TRPC6 or TRPC7 in heterologous expression systems. For example, coexpression of the photopigment melanopsin with homomeric TRPC3 channels in various heterologous expressions systems results in light-evoked conductance increases with the expected spectral properties (Melyan *et al.*, 2005; Panda *et al.*, 2005; Qiu *et al.*, 2005). Pharmacological studies are also supportive that melanopsin activates diacylglycerol-sensitive TRPC channels in the mammalian retina. It has been shown that the membrane permeant analog of diacylglycerol, 1-oleoyl-2-acetyl-sn-glycerol (OAG) moderately potentiates the intrinsic light responses of ipRGCs (Warren *et al.*, 2006)(but see below). Furthermore, studies have shown that several agents known to block TRPC channels can block ipRGC light responses (Warren *et al.*, 2006; Hartwick *et al.*, 2007; Sekaran *et al.*, 2007). Finally, TRPC6 or TRPC7 subunits immunoreactivities have been described in melanopsin-expressing ganglion cells (Warren *et al.*, 2006; Sekaran *et al.*, 2007).

While this hypothesis that melanopsin requires a diacylglycerol-sensitive TRPC channel for phototransduction is generally accepted, some results are difficult to reconcile. For instance, one study finds TRPC6 expression principally in dendrites and soma of ipRGCs (Warren *et al.*, 2006) while another study reports its preferential nuclear localization (Sekaran *et al.*, 2007) casting doubts on the specificity of currently available antibodies. Moreover, TRPC7 was suggested as a candidate for the melanopsin transducing channel because of its relative enrichment in ipRGCs to other ganglion cells (Hartwick *et al.*, 2007). However, a recent study has shown that ectopic expression of melanopsin in "regular" RGCs is able to confer upon these RGCs an intrinsic photosensitivity similar to that reported in ipRGCs (Lin *et al.*, 2008). This suggests that melanopsin is able to gate channels, possibly of the TRPC family, that are ubiquitously expressed within the retina and therefore need not be enriched in the ipRGC population to serve as a candidate for melanopsin-mediated phototransduction. Finally, there are contradictory results in regard to the pharmacological evidence for the diacylglycerol sensitivity of melanopsin-transducing channels. A recent study has failed to demonstrate either OAG-induced currents in ipRGCs or occlusion of light-evoked currents in ipRGCs exposed to diacylglycerol analogs (Graham *et al.*, 2008). Thus, a fuller exploration into the role of other TRPC channels in the native ipRGCs may be warranted at this point.

Our results do indicate that TRPC3, TRPC6, TRPC7 subunits are expressed in the retina at P6-P8 and that retinal development seems to proceed as usual in the absence of each of these three TRPC subunits. It was our expectation that at earlier postnatal stages the issues of compensation would be minimized and therefore we would detect large deficits in the light-evoked responses in the mouse null lines. However, MEA recordings from neonatal ipRGCs in *TRPC3−/ −*, *TRPC6−/ −*, and *TRPC7−/ −* mouse lines continued to show robust light-evoked increases with half-maximal responses (IR_{50})similar to those recorded in WT mice. We did observe a significant decrease in spike frequency attained at several light intensities in *TRPC3−/ −* mice. Single cell recordings from adult ipRGCs allowed us to address the question whether lack of expression of specific TRPC channels affects differentially M1 or M2 ipRGC subtypes with regard to their intrinsic light responses. We found that lack of TRPC3 or TRPC7 subunit expression did not induce significant changes in the intrinsic light responses of either M1 or M2 cells. Interestingly in the *TRPC6−/ −* adult mice, the melanopsin-evoked currents and membrane depolarizations were substantially smaller than those recorded in age-matched WT mice. Together, these findings indicate subtle changes in the ipRGC light responses across the analyzed *TRPC3−/ −*, *TRPC6−/ −*, and *TRPC7−/ −* mouse lines and again were not supportive of the notion that melanopsin promotes depolarization of ipRGCs by activation of homomeric TRPC3/6/7 ion channels. The results gathered in the *TRPC6−/ −* mice are however suggestive that the phototransduction channel does include TRPC6 subunits, at least in mature retinas.

Although issues of developmental compensation may complicate the interpretation of our data, the most parsimonious explanation for the previous accounts and our results is to consider that TRPC7 and TRPC3 homomeric channels do not constitute the long sought transduction channels in ipRGCs. Alternatively, these subunits may do so by forming heteromultimeric assemblies among themselves or with other unidentified TRPC channels. For instance, TRPC3 subunits have recently been shown to heteromultimerize with TRPC1 subunits in smooth muscle cells (Chen *et al.*, 2009) and a similar scenario may apply to ipRCGs. Further works, and in particular a better biophysical characterization and usage of compound TRPC knockout mouse lines, should help to decipher the molecular nature of the transducing channel in ipRGCs.

Supplementary Material

Refer to Web version on PubMed Central for supplementary material.

Acknowledgments

ABBREVIATIONS

EGFP	Enhanced Green Fluorescent Protein
ES	Embryonic Stem Cells
GCL	Ganglion Cell Layer
IPL	Inner Plexiform Layer
ipRGCs	Intrinsically Photosensitive Retinal Ganglion Cells
MEA	Multi Electrode Array
NIF	Non-Image Forming
OAG	diacylglycerol,1-oleoyl-2-acetyl-sn-glycerol
ONL	Outer Nuclear Layer
Opn4	Melanopsin
PCR	Polymerase Chain Reaction
TRPC	Canonical Transient Receptor Potential Channel
WT	Wild-Type

References

Acosta ML, Bumsted O'Brien KM, Tan SS, Kalloniatis M. Emergence of cellular markers and functional ionotropic glutamate receptors on tangentially dispersed cells in the developing mouse retina. J Comp Neurol. 2008; 506:506–523. [PubMed: 18041773]

Baver SB, Pickard GE, Sollars PJ, Pickard GE. Two types of melanopsin retinal ganglion cell differentially innervate the hypothalamic suprachiasmatic nucleus and the olivary pretectal nucleus. Eur J Neurosci. 2008; 27:1763–1770. [PubMed: 18371076]

Berson DM. Phototransduction in ganglion-cell photoreceptors. Pflugers Arch. 2007; 454:849–855. [PubMed: 17351786]

Berson DM, Dunn FA, Takao M. Phototransduction by retinal ganglion cells that set the circadian clock. Science. 2002; 295:1070–1073. [PubMed: 11834835]

Birnbaumer L. The TRPC Class of Ion Channels: A Critical Review of Their Roles in Slow, Sustained Increases in Intracellular Ca(2+) Concentrations (*). Annu Rev Pharmacol Toxicol. 2009; 49:395–426. [PubMed: 19281310]

Chen J, Crossland RF, Noorani MM, Marrelli SP. Inhibition of TRPC1/TRPC3 by PKG contributes to NO-mediated vasorelaxation. Am J Physiol Heart Circ Physiol. 2009; 297:H417–424. [PubMed: 19502552]

Clapham DE, Runnels LW, Strubing C. The TRP ion channel family. Nat Rev Neurosci. 2001; 2:387–396. [PubMed: 11389472]

Connors NC, Kofuji P. Dystrophin Dp71 is critical for the clustered localization of potassium channels in retinal glial cells. J Neurosci. 2002; 22:4321–4327. [PubMed: 12040037]

Dacey DM, Liao HW, Peterson BB, Robinson FR, Smith VC, Pokorny J, Yau KW, Gamlin PD. Melanopsin-expressing ganglion cells in primate retina signal colour and irradiance and project to the LGN. Nature. 2005; 433:749–754. [PubMed: 15716953]

Dietrich A, Mederos YSM, Gollasch M, Gross V, Storch U, Dubrovska G, Obst M, Yildirim E, Salanova B, Kalwa H, Essin K, Pinkenburg O, Luft FC, Gudermann T, Birnbaumer L. Increased vascular smooth muscle contractility in TRPC6−/ −mice. Mol Cell Biol. 2005; 25:6980–6989. [PubMed: 16055711]

Do MT, Yau KW. Intrinsically photosensitive retinal ganglion cells. Physiol Rev. 2010; 90:1547–1581. [PubMed: 20959623]

Ecker JL, Dumitrescu ON, Wong KY, Alam NM, Chen SK, LeGates T, Renna JM, Prusky GT, Berson DM, Hattar S. Melanopsin-expressing retinal ganglion-cell photoreceptors: cellular diversity and role in pattern vision. Neuron. 2010; 67:49–60. [PubMed: 20624591]

Edgington, ES.; Onghena, P. Randomization tests. Chapman & Hall/CRC; Boca Raton, FL: 2007.

Gaillard F, Bonfield S, Gilmour GS, Kuny S, Mema SC, Martin BT, Smale L, Crowder N, Stell WK, Sauve Y. Retinal anatomy and visual performance in a diurnal cone-rich laboratory rodent, the Nile grass rat (Arvicanthis niloticus). J Comp Neurol. 2008; 510:525–538. [PubMed: 18680202]

Goz D, Studholme K, Lappi DA, Rollag MD, Provencio I, Morin LP. Targeted destruction of photosensitive retinal ganglion cells with a saporin conjugate alters the effects of light on mouse circadian rhythms. PLoS One. 2008; 3:e3153. [PubMed: 18773079]

Graham DM, Wong KY, Shapiro P, Frederick C, Pattabiraman K, Berson DM. Melanopsin ganglion cells use a membrane-associated rhabdomeric phototransduction cascade. J Neurophysiol. 2008; 99:2522–2532. [PubMed: 18305089]

Guler AD, Ecker JL, Lall GS, Haq S, Altimus CM, Liao HW, Barnard AR, Cahill H, Badea TC, Zhao H, Hankins MW, Berson DM, Lucas RJ, Yau KW, Hattar S. Melanopsin cells are the principal conduits for rod-cone input to non-image-forming vision. Nature. 2008; 453:102–105. [PubMed: 18432195]

Hardie RC, Minke B. The trp gene is essential for a light-activated Ca2+ channel in Drosophila photoreceptors. Neuron. 1992; 8:643–651. [PubMed: 1314617]

Hardie RC, Raghu P. Visual transduction in Drosophila. Nature. 2001; 413:186–193. [PubMed: 11557987]

Hartmann J, Dragicevic E, Adelsberger H, Henning HA, Sumser M, Abramowitz J, Blum R, Dietrich A, Freichel M, Flockerzi V, Birnbaumer L, Konnerth A. TRPC3 channels are required for synaptic transmission and motor coordination. Neuron. 2008; 59:392–398. [PubMed: 18701065]

Hartwick AT, Bramley JR, Yu J, Stevens KT, Allen CN, Baldridge WH, Sollars PJ, Pickard GE. Light-evoked calcium responses of isolated melanopsin-expressing retinal ganglion cells. J Neurosci. 2007; 27:13468–13480. [PubMed: 18057205]

Hatori M, Le H, Vollmers C, Keding SR, Tanaka N, Schmedt C, Jegla T, Panda S. Inducible ablation of melanopsin-expressing retinal ganglion cells reveals their central role in non-image forming visual responses. PLoS ONE. 2008; 3:e2451. [PubMed: 18545654]

Hattar S, Kumar M, Park A, Tong P, Tung J, Yau KW, Berson DM. Central projections of melanopsin-expressing retinal ganglion cells in the mouse. J Comp Neurol. 2006; 497:326–349. [PubMed: 16736474]

Hattar S, Liao HW, Takao M, Berson DM, Yau KW. Melanopsin-containing retinal ganglion cells: architecture, projections, and intrinsic photosensitivity. Science. 2002; 295:1065–1070. [PubMed: 11834834]

Haverkamp S, Wassle H. Immunocytochemical analysis of the mouse retina. J Comp Neurol. 2000; 424:1–23. [PubMed: 10888735]

Hofmann T, Schaefer M, Schultz G, Gudermann T. Subunit composition of mammalian transient receptor potential channels in living cells. Proc Natl Acad Sci U S A. 2002; 99:7461–7466. [PubMed: 12032305]

Kim IJ, Zhang Y, Yamagata M, Meister M, Sanes JR. Molecular identification of a retinal cell type that responds to upward motion. Nature. 2008; 452:478–482. [PubMed: 18368118]

Li Y, Jia YC, Cui K, Li N, Zheng ZY, Wang YZ, Yuan XB. Essential role of TRPC channels in the guidance of nerve growth cones by brain-derived neurotrophic factor. Nature. 2005; 434:894–898. [PubMed: 15758952]

Lin B, Koizumi A, Tanaka N, Panda S, Masland RH. Restoration of visual function in retinal degeneration mice by ectopic expression of melanopsin. Proc Natl Acad Sci U S A. 2008; 105:16009–16014. [PubMed: 18836071]

Melyan Z, Tarttelin EE, Bellingham J, Lucas RJ, Hankins MW. Addition of human melanopsin renders mammalian cells photoresponsive. Nature. 2005; 433:741–745. [PubMed: 15674244]

Neumann T, Ziegler C, Blau A. Multielectrode array recordings reveal physiological diversity of intrinsically photosensitive retinal ganglion cells in the chick embryo. Brain Res. 2008; 1207:120–127. [PubMed: 18377877]

Nickle B, Robinson PR. The opsins of the vertebrate retina: insights from structural, biochemical, and evolutionary studies. Cell Mol Life Sci. 2007; 64:2917–2932. [PubMed: 17726575]

Panda S, Nayak SK, Campo B, Walker JR, Hogenesch JB, Jegla T. Illumination of the melanopsin signaling pathway. Science. 2005; 307:600–604. [PubMed: 15681390]

Peirson SN, Oster H, Jones SL, Leitges M, Hankins MW, Foster RG. Microarray analysis and functional genomics identify novel components of melanopsin signaling. Curr Biol. 2007; 17:1363–1372. [PubMed: 17702581]

Pfaffl MW. A new mathematical model for relative quantification in real-time RT-PCR. Nucleic Acids Res. 2001; 29:e45. [PubMed: 11328886]

Phillips AM, Bull A, Kelly LE. Identification of a Drosophila gene encoding a calmodulin-binding protein with homology to the trp phototransduction gene. Neuron. 1992; 8:631–642. [PubMed: 1314616]

Qiu X, Kumbalasiri T, Carlson SM, Wong KY, Krishna V, Provencio I, Berson DM. Induction of photosensitivity by heterologous expression of melanopsin. Nature. 2005; 433:745–749. [PubMed: 15674243]

Rudolph U, Bradley A, Birnbaumer L. Targeted inactivation of the Gi2 alpha gene with replacement and insertion vectors: analysis in a 96-well plate format. Methods Enzymol. 1994; 237:366–386. [PubMed: 7935011]

Schmidt TM, Kofuji P. Functional and morphological differences among intrinsically photosensitive retinal ganglion cells. J Neurosci. 2009; 29:476–482. [PubMed: 19144848]

Schmidt TM, Kofuji P. Differential cone pathway influence on intrinsically photosensitive retinal ganglion cell subtypes. J Neurosci. 2010a In press.

Schmidt TM, Kofuji P. An isolated retinal preparation to record light responses from genetically labeled retinal ganglion cells. J Vis Exp. 2010b In press.

Schmidt TM, Taniguchi K, Kofuji P. Intrinsic and extrinsic light responses in melanopsin-expressing ganglion cells during mouse development. J Neurophysiol. 2008; 100:371–384. [PubMed: 18480363]

Sekaran S, Foster RG, Lucas RJ, Hankins MW. Calcium imaging reveals a network of intrinsically light-sensitive inner-retinal neurons. Curr Biol. 2003; 13:1290–1298. [PubMed: 12906788]

Sekaran S, Lall GS, Ralphs KL, Wolstenholme AJ, Lucas RJ, Foster RG, Hankins MW. 2-Aminoethoxydiphenylborane is an acute inhibitor of directly photosensitive retinal ganglion cell activity in vitro and in vivo. J Neurosci. 2007; 27:3981–3986. [PubMed: 17428972]

Sekaran S, Lupi D, Jones SL, Sheely CJ, Hattar S, Yau KW, Lucas RJ, Foster RG, Hankins MW. Melanopsin-dependent photoreception provides earliest light detection in the mammalian retina. Curr Biol. 2005; 15:1099–1107. [PubMed: 15964274]

Sernagor E, Eglen SJ, Wong RO. Development of retinal ganglion cell structure and function. Prog Retin Eye Res. 2001; 20:139–174. [PubMed: 11173250]

Sun C, Speer CM, Wang GY, Chapman B, Chalupa LM. Epibatidine application in vitro blocks retinal waves without silencing all retinal ganglion cell action potentials in developing retina of the mouse and ferret. J Neurophysiol. 2008; 100:3253–3263. [PubMed: 18922954]

Tai Y, Feng S, Du W, Wang Y. Functional roles of TRPC channels in the developing brain. Pflugers Arch. 2009; 458:283–289. [PubMed: 19023589]

Tu DC, Zhang D, Demas J, Slutsky EB, Provencio I, Holy TE, Van Gelder RN. Physiologic diversity and development of intrinsically photosensitive retinal ganglion cells. Neuron. 2005; 48:987–999. [PubMed: 16364902]

Viney TJ, Balint K, Hillier D, Siegert S, Boldogkoi Z, Enquist LW, Meister M, Cepko CL, Roska B. Local retinal circuits of melanopsin-containing ganglion cells identified by transsynaptic viral tracing. Curr Biol. 2007; 17:981–988. [PubMed: 17524644]

Warren EJ, Allen CN, Brown RL, Robinson DW. The light-activated signaling pathway in SCN-projecting rat retinal ganglion cells. Eur J Neurosci. 2006; 23:2477–2487. [PubMed: 16706854]

Weng S, Wong KY, Berson DM. Circadian modulation of melanopsin-driven light response in rat ganglion-cell photoreceptors. J Biol Rhythms. 2009; 24:391–402. [PubMed: 19755584]

Young S, Rothbard J, Parker PJ. A monoclonal antibody recognising the site of limited proteolysis of protein kinase C. Inhibition of down-regulation in vivo. Eur J Biochem. 1988; 173:247–252. [PubMed: 2451608]

Zhang J, Yang Z, Wu SM. Development of cholinergic amacrine cells is visual activity-dependent in the postnatal mouse retina. J Comp Neurol. 2005; 484:331–343. [PubMed: 15739235]
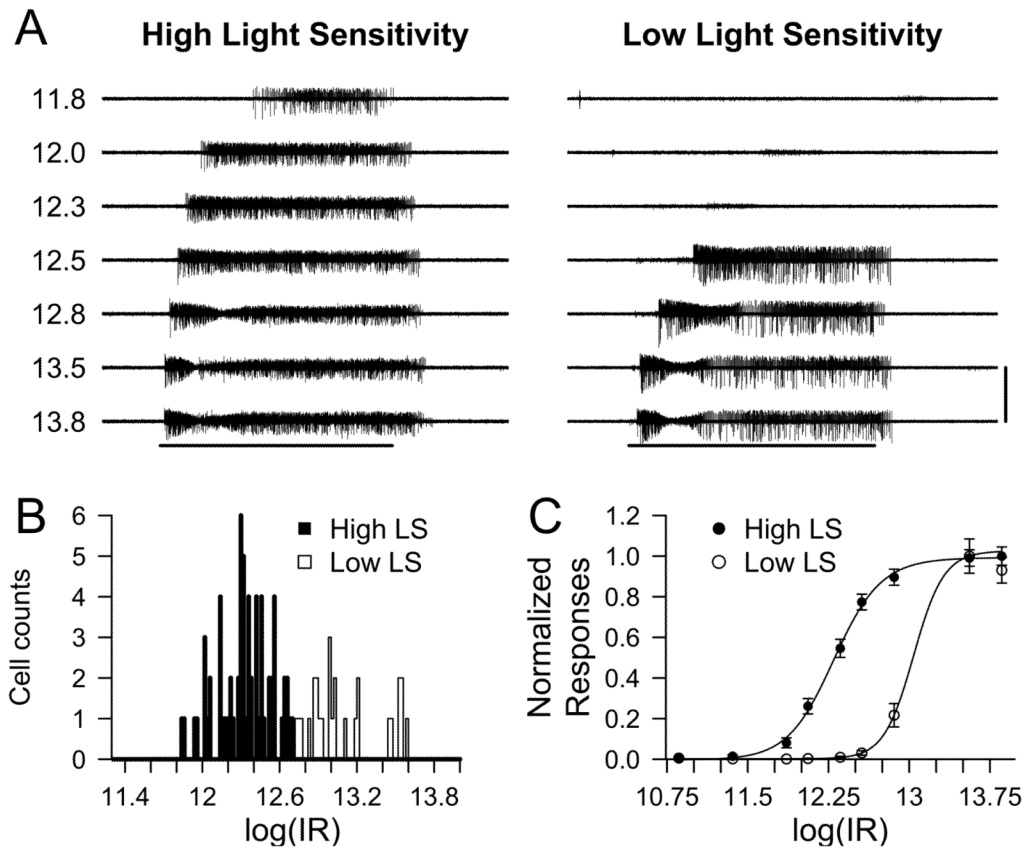
Figure 1. Intrinsic light responses of P6-P8 WT ipRGCs
A) Representative voltage traces for high light sensitivity (LS) and low LS ipRGCs obtained using MEA recording. Numbers on the left of the traces indicate the logarithmic of light stimulation intensity in photons / $cm^2 \cdot$ sec. Horizontal bar indicates 480 nm light stimulus with duration of 60 sec. Vertical bar represents 300 µV. **B)** Histogram of $log(IR_{50})$ values (in photons / $cm^2 \cdot$ sec) for ipRGC intrinsic light responses calculated from the Hill Function fit over normalized light induced spikes. High and low LS responses were separated at $log(IR_{50}) = 12.70$. **C)** Dose-response graph of the normalized light responses (mean ± SEM) and the fitted Hill function for high ($log(IR_{50}) = 12.30$ in photons / $cm^2 \cdot$ sec) and low ($log(IR_{50}) = 13.04$ photons / $cm^2 \cdot$ sec) LS ipRGCs.
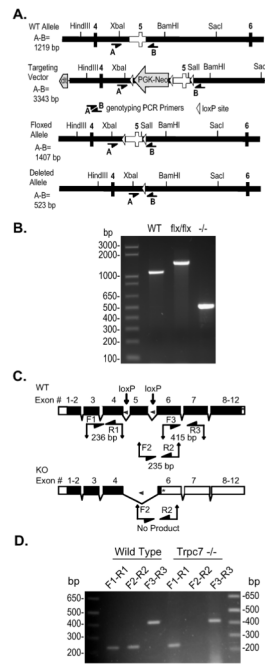
Figure 2. Disruption of the murine *TRPC7* locus

A) Targeting strategy. WT Allele: depicts the region of the wild type *TRPC7* gene containing the targeted exon 5 (clear) used to construct the targeting vector. Targeting Vector: depicts the portion of the targeting vector used to target the *TRPC7* locus by homologous recombination. Floxed Allele: depicts the structure of the targeted allele after Cre-mediated excision of the PGK-Neo cassette with exon 5 flanked by loxP sites. Deleted Allele: depicts the structure of the disrupted allele from which exon 5 has been removed by the action of Cre recombinase. The position of key restriction endonuclease sites and the location of genotyping primers A (5'-CCTTC CTCTC TAGGT TCCTT CTAG) and B (5'-GTAGT ATCAG GAAGC TCGCG GCTCT) are indicated. Rectangles, exons included in targeting vector; heavy black line, intronic sequence included in the targeting vector; open triangle, loxP site; PGK-Neo, neomycin selection cassette; dt, diptheria toxin selection cassette. **B)** PCR analysis of mouse genomic DNA using primers A and B. F1 recombinant mice (flx/WT) were interbred, and then bred to Sox2-Cre mice (Jackson Laboratories) to promote excision of exon 5, and then interbred to generate exon 5 null mice that had also lost the cre transgene. All *TRPC7* genotypes produce PCR products of the expected sizes given in A. WT, DNA from wild-type mouse; flx/flx, DNA from mouse homozygous for the floxed allele; −/ −, DNA from mouse homozygous for the deleted allele which exon 5 has been excised by a Cre transgene driven by the uniquitous *Sox2* promoter. **C)** (Top) Diagram of the wild-type intron/exon organization of the *TRPC7* gene. Locations of loxP sites in the floxed allele and RT-PCR primers are indicated. (Bottom) Diagram of the deleted allele. Deletion of exon 5 by Cre recombinase is predicted to result in a frameshift and premature stop codon in exon 6. The lengths of the depicted amplicons include the primers. Primer F1 (5'-ATGTG AACTT GCAAG TCTGG TCCG), R1 (5'-AGCAA TCCAA TAGGC TATGG CGAG), F2 (5'-GACGG AGATG CTCAT CATGA AGTG), R2 (5'-TGAGA CGTTG TGCAG CGTTA CATC), F3 (5'-TGCTA CACTT GTGGA ACCTT CTGG), R3 (5'-CGGTA GTAGG AGTAC AGGTT GAAC). Black boxes, coding sequence; open boxes, untranslated exon sequence; *, stop codon. **D)** RT-PCR analysis of brain RNA from a wild-type and a *TRPC7−/ −*mouse. Primer pairs are indicated, their position in the gene and predicted product sizes are given in C. Sequencing of the RT-PCR products confirmed

splicing from exon 4 to exon 6 and the presence of a premature stop codon in mRNA transcribed from the deleted allele.
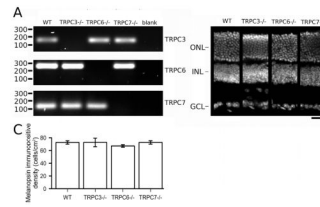
Figure 3. Characterization of *TRPC3−/−*, *TRPC6−/−* and *TRPC7−/−* retinas
A) End-point RT-PCR analysis from adult retinal samples shows the absence of respective ablated exons in *TRPC3−/−*, *TRPC6−/−* and *TRPC7−/−* retinal transcripts. RT-PCR for TRPC3 exon 7 (145 bp), TRPC6 exon 7 (247 bp), TRPC7 exon 5 (110 bp) shows the presence in WT retinas but not in the respective mutant mouse line samples. Blank controls are RT-PCR reactions with H_2O instead of cDNAs. **B)** Cross sections of DAPI stained adult retinas show apparent normal morphology in *TRPC3−/−*, *TRPC6−/−* and *TRPC7−/−* mice compared to WT mice (scale bar 20 μm). **C)** Densities of melanopsin immunoreactive cell bodies in WT, *TRPC3−/−*, *TRPC6−/−,* and *TRPC7−/−* mouse retinas (mean ± SEM). ONL, outer nuclear layer; INL, inner nuclear layer; GCL, ganglion cell layer.
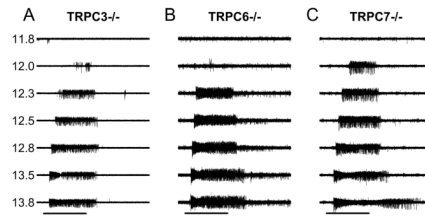
Figure 4. Intrinsic light responses of *TRPC3−/−*, *TRPC6−/−* and *TRPC7−/−* ipRGCs
Representative voltage traces for ipRGC intrinsic light responses in *TRPC3−/−* (**A**),
TRPC6−/− (**B**) and *TRPC7−/−* (**C**) retinas. Numbers on the left of the traces indicate the
logarithmic of light stimulation intensity in photons / cm² · sec. Horizontal bar represents
light stimulation (60 sec). Vertical scale bar is 300 µV. Each one of the traces represents the
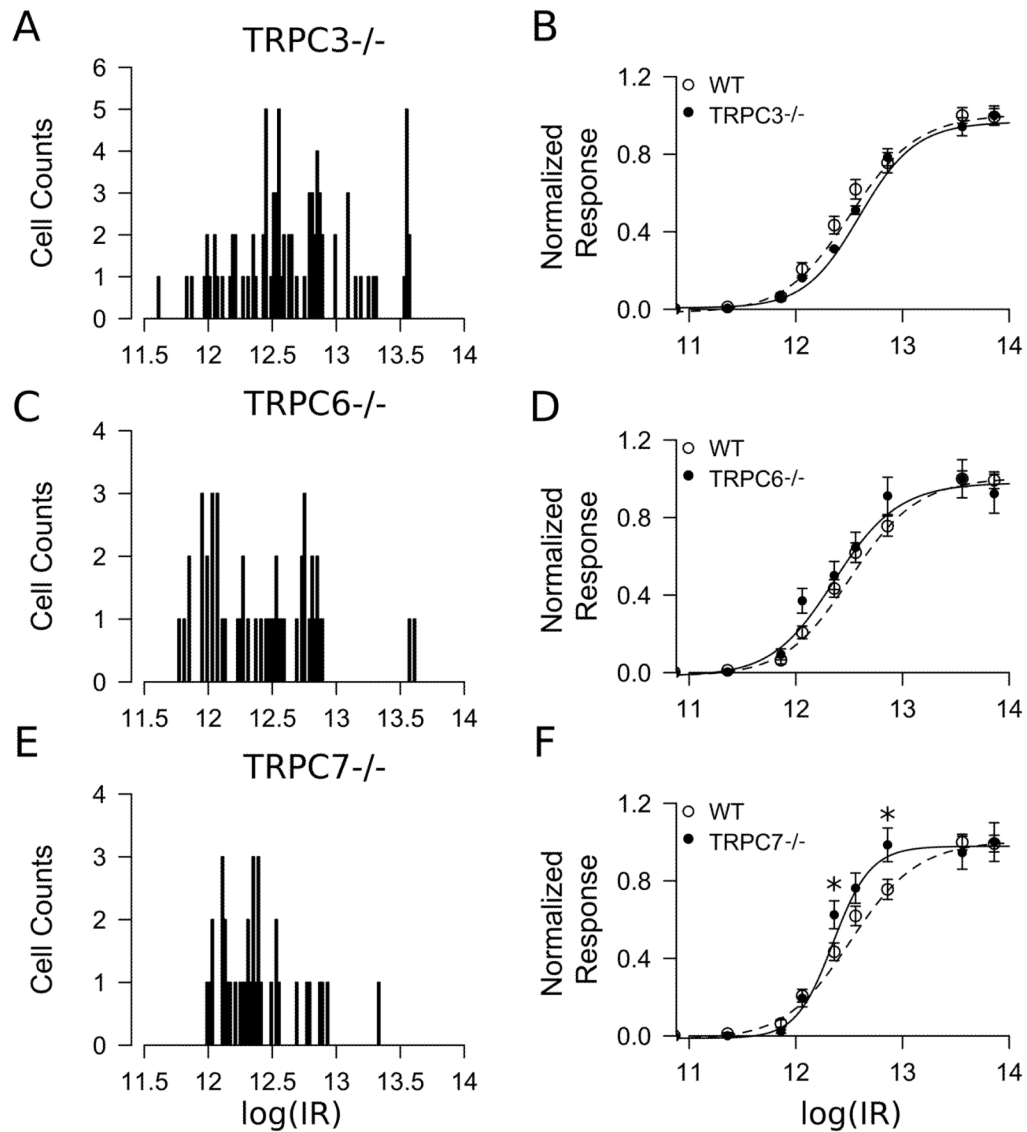light response at a given 480 nm light intensity.

Figure 5. Summary of intrinsic light responses in *TRPC3−/−*, *TRPC6−/−* and *TRPC7−/−* ipRGCs

(A,C,E)

Histograms of the $\log(IR_{50})$ in photons $/ \, cm^2 \cdot$ sec for (A) *TRPC3−/−* ($n = 84$ cells), (C) *TRPC6−/−* ($n = 49$ cells) and (E) *TRPC7−/−* ($n = 37$ cells) ipRGC light responses. (**B,D,F**) Normalized light responses (mean ± SEM) and the fitted Hill function for (B) *TRPC3−/−* ($\log(IR_{50}) = 12.52$), (D) *TRPC6−/−* ($\log(IR_{50}) = 12.30$) and (F) *TRPC7−/−* ($\log(IR_{50}) = 12.28$). The WT normalized light response shown here was calculated using all WT ipRGC responses ($n = 93$, $\log(IR_{50}) = 12.44$).
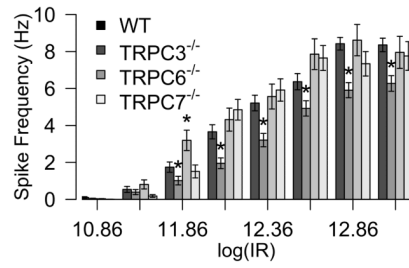
Figure 6. Irradiance-response relationships for WT, *TRPC3−/ −*, *TRPC6−/ −* and *TRPC7−/ −* ipRGCs
Average spike frequency in WT and mutant mice ipRGCs recorded at various light intensities (Log photons/cm^2.s). Significant differences were recorded across various light intensities for *TRPC3−/ −* retinas and one light intensity for *TRPC6−/ −* retinas. * indicates *P* value < 0.05 in a randomization based t-test comparing WT and the corresponding TRPC −/ − response at each light intensity after a FDR correction for multiple comparisons.
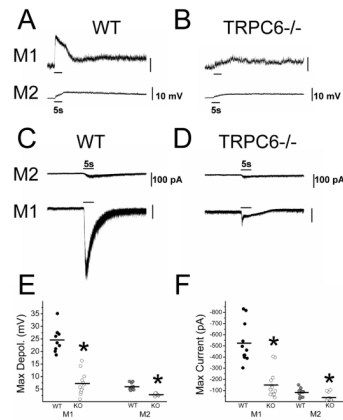
Figure 7. Current and voltage clamp recordings of light responses of M1 and M2 ipRGCs in WT and *TRPC6−/ −* mice

(A) Representative intrinsic light responses of M1 (top trace) and M2 (bottom trace) cells in adult WT mice to a 5 s full-field 480 nm light stimulus at −2.1LogI recorded in current clamp mode. **(B)** Representative intrinsic light responses of M1 (top trace) and M2 (bottom trace) cells in adult *TRPC6−/ −* mice to a 5 s full-field 480 nm light stimulus at −2.1LogI recorded in current clamp mode. **(C)** Representative intrinsic light response of M2 (top trace) and M1 (bottom trace) cells in adult WT mice to a 5 s full-field 480 nm light stimulus at − 1.5LogI recorded in voltage clamp mode (V_{hold} −80mV). **(D)** Representative intrinsic light response of M2 (top trace) and M1 (bottom trace) cells in adult *TRPC6−/ −* mice to a 5 s full-field 480 nm light stimulus at −1.5LogI recorded in voltage clamp mode (V_{hold} −80mV). **(E)** Maximum depolarization evoked by a 5s full-field 480 nm light stimulation in WT and *TRPC6−/ −* M1 and M2 cells. Black bars indicate mean. **(F)** Maximum inward current evoked by a 5 s full-field 480 nm light stimulus in WT and *TRPC6−/ −* M1 and M2 cells. Black bars indicate mean. * $P < 0.05$, two-tailed *t*-test.
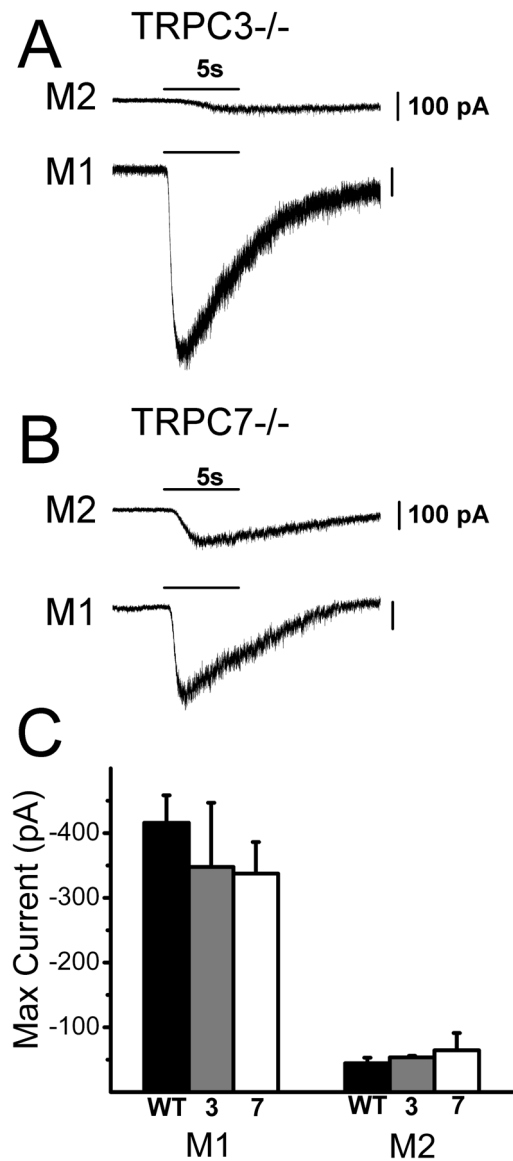
Figure 8. Voltage clamp recordings of light responses of M1 and M2 ipRGCs in *TRPC3−/ −*and *TRPC7−/ −* mice

(A) Representative intrinsic light response of M2 (top trace) and M1 (bottom trace) cells in adult *TRPC3−/ −* mice to a 5 s full-field 480 nm light stimulus at −1.5LogI recorded in voltage clamp mode (V_{hold} -60mV). **(B)** Representative intrinsic light response of M2 (top trace) and M1 (bottom trace) cells in adult *TRPC7−/ −* mice to a 5 s full-field 480 nm light stimulus at −1.5LogI recorded in voltage clamp mode (V_{hold} -60mV). **(C)** Mean ± SE maximum inward current to a 5 s full-field 480 nm light stimulus in WT, *TRPC3−/ −*, and *TRPC7−/ −* M1 and M2 cells (V_{hold} −60mV).

Table 1

Primary antibodies used in this study.

Antibody against	Host	Dilution	Immunogen	Specificity	Reference	Source	Catalog number	Retina reference
Glutamine synthetase	Mouse	1:400	Sheep enzyme 1–373	Western bolot 45 kDa	Manufacturer	BD Biosciences	610518	(Zhang *et al.*, 2005)
Protein kinase C-α	Mouse	1:400	Purified bovine brain PKC, amino acids 296–317	Western blot 80KDa	(Young *et al.*, 1988)	Abcam	Ab31	(Kim *et al.*, 2008)
choline acetyl transferase	Goat	1:200	human placental enzyme	Western blot 70KDa	Manufacturer	Millipore	Ab144p	(Gaillard *et al.*, 2008)
Tyrosine hydroxylase	Rabbit	1:400	tyrosine hydroxylase from rat pheochromocyt oma (	Western blot 62kDa	Manufacturer	Millipore	Ab152	(Acosta *et al.*, 2008)
Melanopsin	Rabbit	1:500	1–19 aa mouse melanopsin	*		Home made		

*Specificity of anti-melanopsin antibody was tested upon immunostaining in WT, and *Opn4−/−*mouse retinas (see methods).

Table 2

Analysis of ipRGC intrinsic light responses in WT P6-P8 retinas.

log (IR)	Average Spike frequency(Hz)		Maximal Spike Frequency(Hz)		Latency to Maximal Spike Frequency(s)	
	High LS**	Low LS	High LS	Low LS	High LS	Low LS
12.56	7.27 ± 0.37	0.19 ± 0.07 *	10.96 ± 0.51	0.43 ± 0.15 *	14.39 ± 0.65	40 ± 6.07 (n=7) *
12.86	8.42 ± 0.37	1.36 ± 0.36 *	12.66 ± 0.68	2.72 ± 0.62 *	9.62 ± 0.59	34.17 ± 8.88 (n=18) *
13.56	9.31 ± 0.38	6.26 ± 0.53 *	14.85 ± 0.72	8.61 ± 0.63 *	7.12 ± 0.82	18.33 ± 2.28
13.86	9.39 ± 0.42	5.83 ± 0.40 *	14.78 ± 0.74	7.54 ± 0.57 *	5.83 ± 0.64	15.93 ± 1.36

**
High LS, High and Low light sensitive (LS) groups as defined by a cutoff of $\log(IR) = 12.70$ photons / $cm^2 \cdot$ sec (see results section)

*
Represents significant values (P<0.05) when comparisons are made between the High and Low LS groups.